Nematic wetting layers in liquid crystal colloids

2004 J. Phys.: Condens. Matter 16 S1911

(http://iopscience.iop.org/0953-8984/16/19/004)

INSTITUTE OF PHYSICS PUBLISHING JOURNAL OF PHYSICS: CONDENSED MATTER

J. Phys.: Condens. Matter **16** (2004) S1911–S1919 PII: S0953-8984(04)73709-1

Nematic wetting layers in liquid crystal colloids

Holger Stark[1], **Jun-ichi Fukuda**[2] **and Hiroshi Yokoyama**[2,3]

[1] Universität Konstanz, Fachbereich Physik, Fach M621, D-78467 Konstanz, Germany
[2] Yokoyama Nano-structured Liquid Crystal Project, ERATO, Japan Science and Technology Corporation, 5-9-9 Tokodai, Tsukuba 300-2635, Japan
[3] Nanotechnology Research Institute, AIST, 1-1-4 Umezono, Tsukuba 305-8568, Japan

E-mail: Holger.Stark@uni-konstanz.de

Received 17 December 2003
Published 30 April 2004
Online at stacks.iop.org/JPhysCM/16/S1911
DOI: 10.1088/0953-8984/16/19/004

Abstract

We first review the method of treating nematic wetting of planar surfaces following the approach introduced by Sheng. We present a phase diagram, which in the present form we have not found in the original literature. Then we consider spherical geometries of arbitrary radii, such as colloidal particles, and introduce an appropriate method for handling wetting in curved geometries. We find that a prewetting transition for high curvatures or small particle radii no longer occurs.

(Some figures in this article are in colour only in the electronic version)

1. Introduction

The wetting of surfaces by a fluid has tremendous industrial applications. The famous Lotus effect [1] serves as the best example of 'non-wetting': for example, on the basis of this effect self-cleaning wallpaper has been introduced [1]. In 1977 Cahn published a very influential paper in which he studied perfect or complete wetting and prewetting on the basis of mean-field theory [2]. He showed that a two-phase system in contact with a wall moving along the coexistence line towards its critical point exhibits complete wetting beyond the wetting temperature T_w. This is illustrated for a liquid–gas system in figure 1. For example, if the wall induces a film of liquid order, its thickness becomes infinite for temperatures above T_w. Furthermore, a prewetting line exists which starts on the coexistence curve at T_w and, in the present example, ends in a critical point located in the region of the gaseous phase. When crossing the prewetting line, the thickness of the wetting film shows a discontinuity. Wetting has been intensively investigated for three decades now [3, 4]. Cahn's work was extended [5–7] and then wetting of curved surfaces of cylinders and spheres was studied [8, 9], also within density-functional theory [10].

Surface phenomena and the anchoring of the mesogenic molecules on bounding surfaces play a central role in liquid crystal studies due to their technological importance in liquid

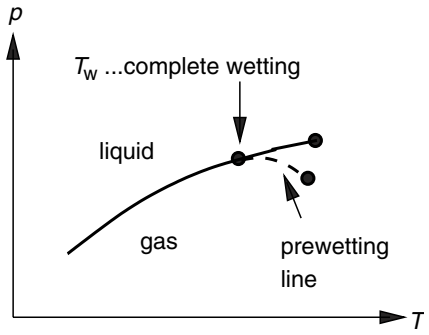

Figure 1. A system at the liquid–gas coexistence line close to a bounding wall exhibits complete wetting when moving towards its critical point beyond the so-called wetting temperature T_w. If the wall favours the liquid phase, a prewetting line extents into the gaseous phase and ends in a critical point.

crystal displays. For a review and an extensive list of references see [11, 12]. Sheng was the first to study prewetting transitions in nematic liquid crystals close to a planar substrate and above the nematic–isotropic phase transition [13]; he called them boundary-layer transitions. Detailed investigations were then performed by Poniewierski and Sluckin [14, 15] who also elaborated on the connection to wetting.

In our work on liquid crystal colloids we are currently exploring the effect of nematic wetting layers around colloidal particles which form above the nematic–isotropic phase transition. We know that they can induce novel colloidal interactions [16–20] which influence the stability of colloidal dispersions. If the radial anchoring of the molecules at the surfaces of the colloidal particles is weak, the particles are surrounded by nematic coronas, whose thickness is given by the nematic coherence length. As a result, the interaction potential is of Yukawa type [17, 19, 20]. This is in close analogy to the Debye–Hückel approximation for electrostatically stabilized colloids [21, 20]. On the other hand, for strong surface anchoring capillary condensation occurs where a bridge of condensed nematic phase forms between the particles. The phenomenon is also called capillary nematization. Now the resulting interaction potential has a larger range, and close to the transition temperature it is approximately linear in the particle distance [18, 22]. A further effect of nematic wetting layers is that they certainly alter the Brownian motion of particles, since a wetting layer changes the friction coefficient in comparison to the conventional Stokes drag in isotropic fluids [23].

In this paper we first review the method to treat nematic wetting of planar surfaces and place it in the context of the language used in wetting science. We present a phase diagram which, in the present form, we have not found in the original literature [6, 7, 14, 15]. Then we show how wetting of spherical particles can be treated [24]. In particular, we demonstrate that for high curvatures or small particle radii a prewetting transition no longer exists. We start with a short summary of Landau–Ginzburg–de Gennes theory.

2. Landau–Ginzburg–de Gennes Theory

This theory is formulated in terms of a traceless second-rank tensor, also called the alignment tensor, which serves as an order parameter to classify orientational order. In a microscopic definition, one describes the direction of single molecules by a unit vector $\hat{\nu}$ and defines the

order parameter as the second moment of the orientational distribution function:

$$Q_{ij} = \langle \hat{\nu}_i \hat{\nu}_j - \tfrac{1}{3}\delta_{ij} \rangle, \tag{1}$$

where $\langle \cdots \rangle$ means average over all molecules in a large enough volume. For a macroscopic definition, one takes any second-rank material tensor $\boldsymbol{M}$, such as the dielectric tensor $\boldsymbol{\varepsilon}$, and extracts the traceless part:

$$Q_{ij} = \frac{3}{\operatorname{tr} \boldsymbol{M}} \left(M_{ij} - \frac{1}{3}\delta_{ij} \operatorname{tr} \boldsymbol{M} \right), \tag{2}$$

where $\operatorname{tr} \boldsymbol{M}$ means the trace of $\boldsymbol{M}$. For uniaxial tensors both definitions are equivalent, however in the case of biaxial order the connection is non-trivial.

In the spirit of Landau and Ginzburg, de Gennes wrote down a free energy functional to treat liquid crystals close to the nematic–isotropic phase transition [25]:

$$F_{\mathrm{LG}}[\boldsymbol{Q}(\boldsymbol{r})] = \int [f_{\mathrm{b}}(\boldsymbol{Q}) + f_{\mathrm{el}}(\nabla \boldsymbol{Q})] \, \mathrm{d}^3 r, \tag{3}$$

where the bulk and elastic free energy densities are

$$f_{\mathrm{b}} = \tfrac{1}{2} a_0 (T - T^*) \operatorname{tr} \boldsymbol{Q}^2 - \tfrac{1}{3} b \operatorname{tr} \boldsymbol{Q}^3 + \tfrac{1}{4} c (\operatorname{tr} \boldsymbol{Q}^2)^2 \tag{4}$$

$$f_{\mathrm{el}} = \tfrac{1}{2} L_1 (Q_{ij,k})^2 + \tfrac{1}{2} L_2 (Q_{ij,i})^2. \tag{5}$$

The symbol $,i$ means the spatial derivative with respect to x_i. The Landau coefficient a_0 is a positive constant to ensure that the symmetry-breaking phase transition takes place when the temperature T is lowered and T^* is the supercooling temperature of the isotropic phase. Furthermore, the following stability conditions have to be fulfilled: $c > 0$, $L_1 > 0$ and $L_1 + \frac{2}{3} L_2 > 0$ [25]. Note that within Landau–de Gennes theory we can only treat orientational wetting. Smectic ordering induced by surfaces is not addressed in this paper.

The bulk free energy density (4) is minimized by a uniaxial order parameter,

$$Q_{ij} = S(n_i n_j - \tfrac{1}{3}\delta_{ij}), \tag{6}$$

where the unit vector $\boldsymbol{n}$ is the director and S is the Maier–Saupe scalar order parameter. The energy density f_{b} then becomes an expansion in S and describes the first-order nematic–isotropic phase transition with prolate ($S > 0$ for $b > 0$) or oblate ($S < 0$ for $b < 0$) orientational order. Surfaces, for example, can induce a non-uniform nematic state, probably with small biaxial contributions. However, in the following we will naturally assume that a surface potential induces homeotropic, uniaxial ordering on a planar and a spherical surface (see below). For symmetry reasons, we then do not expect any biaxial orientational ordering.

Furthermore, we will choose $L_2 = 0$ to simplify our treatment. However, there is a qualitative effect associated with this choice. For $L_2 > 0$, the director $\boldsymbol{n}$ wants to be parallel to a planar nematic–isotropic interface [25]. By setting $L_2 = 0$, both the parallel and homeotropic orientation of $\boldsymbol{n}$ are equivalent. In addition, we will rescale all quantities in the free energy appropriately so that the temperature $\tau \propto a_0(T - T^*)$ is the only relevant parameter in the reduced free energy. The characteristic length scale is the nematic coherence length $\xi_{\mathrm{r}} = \xi_{\mathrm{N}}(T_{\mathrm{NI}}) \approx 10$ nm at the phase transition temperature T_{NI}. We will refer all lengths to $\xi_{\mathrm{r}}/2\sqrt{2}$.

The coupling of the orientational order to the surface is governed by the Nobili–Durand surface free energy [26]:

$$F_{\mathrm{sur}}[\boldsymbol{Q}(\boldsymbol{r})] = \frac{W}{2} \int (Q_{ij} - Q_{ij}^{(0)})^2 \, \mathrm{d}^2 r, \tag{7}$$

where

$$Q_{ij}^{(0)} = S_0 (n_i^{(0)} n_j^{(0)} - \tfrac{1}{3}\delta_{ij}) \tag{8}$$

is the preferred order parameter at the surface. We assume that it is uniaxial and that the preferred direction $\boldsymbol{n}_0$ is always perpendicular to the surface, which means homeotropic anchoring. The surface coupling parameter $\gamma = W\xi_r/2\sqrt{2}L_1$ quantifies the competition between surface and elastic free energy. Together with S_0 it will appear as an additional free parameter in the following considerations.

3. Nematic wetting: planar geometry

We assume a uniaxial order parameter with a uniform director field in the semi-infinite space bounded by a plane at $z = 0$. Then the reduced bulk free energy reads

$$f_b = \tau S^2 - \frac{1}{\sqrt{6}}S^3 + \frac{1}{3}S^4 \tag{9}$$

and the total free energy per area including the surface energy becomes

$$F_A[S(\boldsymbol{r})] = \int_0^\infty \left[f_b + \left(\frac{d}{dz} S \right)^2 \right] dz + \gamma [S(z=0) - S_0]^2. \tag{10}$$

Note that all the quantities are rescaled, although we did not change their notation. By reducing the planar-geometry problem to one involving a scalar order parameter, we have brought it into the class of simple fluid-like systems studied by previous workers (see, e.g., [5–7]). That said, since the free energy (10) is different from the canonical form used in the classical paper by Nakanishi and Fisher [5], we cannot just adopt their wetting phase diagrams. To be concrete, Nakanishi and Fisher use a vector order parameter, such as the magnetization, and as a result a third-order term in the Landau free energy is not allowed, in contrast to equation (9). In addition, they include a first-order term by introducing an external field to treat first-order phase transitions. Such a term is missing in our case. Similarly, while the form of our Landau expansion (10) is a specific case of those considered by Lipowsky and Speth [7], we have been unable to find its phase diagram in their published work.

We are interested in the order-parameter profiles for the boundary condition $S(z \to \infty) = 0$. We especially want to know the behaviour of $S(0)$. The profiles follow from the respective Euler–Lagrange equations for the bulk and the bounding surface:

$$\frac{d^2S}{dz^2} - \frac{1}{2}\frac{df_b(S)}{dS} = 0, \qquad \left.\frac{dS}{dz}\right|_{z=0} = \gamma[S(0) - S_0]. \tag{11}$$

The bulk equation can be integrated once and then combined with the surface equation to yield a formula from which $S(0)$ is determined:

$$\sqrt{f_b(S(0)) - f_b(S(\infty))} = \gamma |S_0 - S(0)|. \tag{12}$$

Note that $f_b(S(\infty)) = 0$ in our case. Figure 2 presents a graphical solution to equation (12). The full and the dashed lines correspond to the left-hand and the right-hand side of equation (12) respectively. In the case presented in the figure, three solutions are found. To decide upon the absolute minimum, we need to calculate the total free energy. Again, from the integration of the bulk Euler–Lagrange equation in equations (11), one ultimately finds

$$F_A[S(\boldsymbol{r})] = \text{constant} + 2\int_{S(\infty)}^{S(0)} \left[\sqrt{f_b(S) - f_b(S(\infty))} - \gamma(S_0 - S) \right] dS. \tag{13}$$

This expression means that the energies of the three different solutions in figure 2 differ by the areas bounded by the solid and the dashed lines. So the middle solution always gives a maximum in the free energy, whereas in the example of figure 2 the respective solutions on the left-hand and right-hand side correspond to the stable and metastable order-parameter profile.

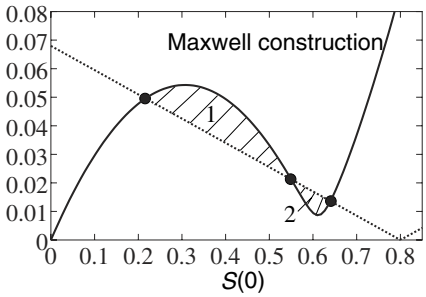

Figure 2. Graphical solution of equation (12). The three intersections are surface values $S(0)$ that belong to order-parameter profiles solving the Euler–Lagrange equations (11). The free energies of these profiles differ by the areas 1 and 2. Here the thin-film solution (smallest $S(0)$) is absolutely stable. If the areas 1 and 2 are the same, a prewetting transition to the thick-film solution (largest $S(0)$) occurs (Maxwell construction).

A phase transition occurs if areas 1 and 2 are both the same, which is the well-known Maxwell construction.

On the basis of such arguments, we constructed the wetting phase diagram in figure 3 in terms of the surface anchoring strength γ, the preferred surface order parameter S_0, and the temperature τ.

The light-grey shaded plane (see figure 3) is situated at the bulk phase-transition temperature τ_b. It gives the parameter region (S_0, γ) where no wetting occurs at all. So when temperature τ decreases towards τ_b, the order parameter always stays in the thin-film solution (lower curve in the inset). Note that for this solution, $S(0)$ always assumes a value smaller than the bulk order parameter S_b at the phase transition. When $S_0 > S_b$ in the parameter region under discussion, (meta)stable thick-film solutions (upper curve in the inset) also exist if τ is close to τ_b. The dark-grey shaded surface gives a qualitative account of the prewetting surface introduced in full analogy to the prewetting line in the introduction. It is determined by the Maxwell construction; however, figure 3 only presents a sketch of it. The prewetting surface is bounded by the dashed and full lines, which we were able to calculate analytically, and extends to temperatures larger than τ_b (see the projection on the (S_0, τ) plane in the figure). When crossing the surface, the boundary-layer transition takes place, i.e. a transition from the thin-film to the thick-film solution (see the inset of figure 3). The prewetting surface ends in a critical line. Here the three solutions of figure 2 merge to the inflection point of the solid curve in figure 2 with the dashed line becoming the tangent. When cooling the system towards τ_b above the critical line, no prewetting occurs and the thickness of the wetting film grows continuously to infinity.

Prewetting lines generally approach coexistence lines tangentially [27]. This is also valid in the present case. This means that the prewetting surface approaches the coexistence plane at $\tau = \tau_b$ such that for constant S_0 the slope $d\gamma/d\tau$ diverges. We have tried to indicate the diverging slope in the cross section of the prewetting surface in figure 3. In analogy to [27], it follows from a Clapeyron-type equation together with the diverging thickness of the thick film for $\tau \to \tau_b$. Let $F_A^{(1)}$ and $F_A^{(2)}$ be the respective free energies of the thin-film $[S_1(z)]$ and the thick-film $[S_2(z)]$ solutions. According to equation (10), their differentials for fixed S_0 but varying τ and γ are

$$dF_A^{(i)} = \left(\int_0^\infty S_i^2 \, dz \right) d\tau + [S_i(0) - S_0]^2 \, d\gamma. \tag{14}$$

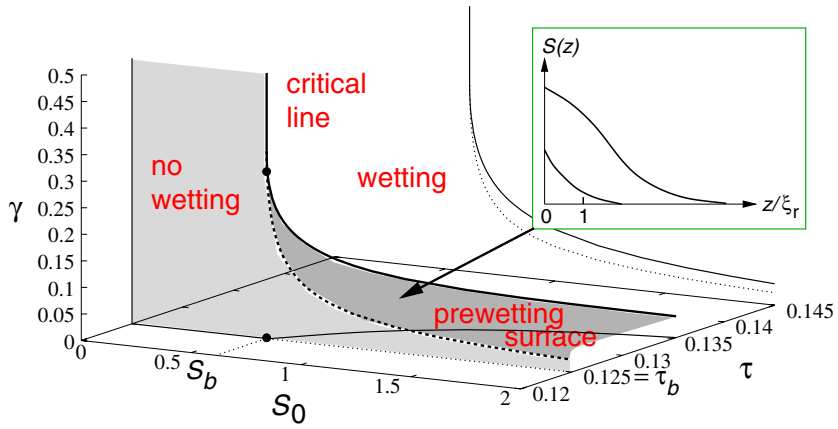

Figure 3. Wetting phase diagram for the planar geometry. In the parameter region (S_0, γ) of the light-grey shaded plane a wetting transition does not occur. The prewetting surface (dark-grey shaded surface) ends in a critical line. The additional full and dotted curves indicate the respective projection of the prewetting surface on the (S_0, τ) plane or the (S_0, γ) plane at $\tau = 0.145$. For a detailed explanation see the text.

The implicit dependence of the order-parameter profiles on τ and γ does not contribute further terms in $\mathrm{d}F_{\mathrm{A}}^{(i)}$ since the profiles satisfy the Euler–Lagrange equations (11). At the prewetting plane $F_{\mathrm{A}}^{(1)} = F_{\mathrm{A}}^{(2)}$, and therefore $\mathrm{d}F_{\mathrm{A}}^{(1)} = \mathrm{d}F_{\mathrm{A}}^{(2)}$. Together with equation (14), this leads to the slope

$$\left.\frac{\mathrm{d}\gamma}{\mathrm{d}\tau}\right|_{S_0=\text{constant}} = -\frac{\int_0^\infty (S_2^2 - S_1^2)\,\mathrm{d}z}{[S_2(0) - S_0]^2 - [S_1(0) - S_0]^2} \tag{15}$$

for the prewetting plane. It diverges weakly when phase coexistence is approached since the thickness of the thick film diverges logarithmically [2].

The present section served to review the formalism for treating wetting phenomena within mean-field theory for a planar geometry. We will contrast it now with the treatment of a curved geometry.

4. Nematic wetting: spherical geometry

We consider a particle of radius a (the reduced value is $\tilde{a} = 2\sqrt{2}a/\xi_{\mathrm{r}}$) which now introduces a second length scale into our system besides the nematic coherence length ξ_{r}. We assume that the molecules prefer homeotropic anchoring at the particle surface and that the order parameter is uniaxial with the director field $\boldsymbol{n}(\boldsymbol{r})$ pointing along the radial direction. Then the reduced free energy as a functional of the scalar order parameter $S(r)$, where r is the reduced radial distance from the centre of the sphere, reads:

$$F[S(r)] = \frac{\xi_{\mathrm{r}}^2}{8a^2}\int_{\tilde{a}}^\infty \mathrm{d}r\, r^2\left[\frac{1}{2}f_{\mathrm{b}} + 3\left(\frac{S}{r}\right)^2 + \frac{1}{2}\left(\frac{\mathrm{d}S}{\mathrm{d}r}\right)^2\right] - wS(\tilde{a}). \tag{16}$$

The bulk free energy f_{b} is the same as in equation (9) and we kept a factor of $1/2$ for convenience. In contrast to the previous section, but in analogy to the original treatment by Sheng [13], we use here a simplified surface potential by just introducing a surface-ordering field w which promotes nematic order for $w > 0$. Note that compared with the planar case, the additional term $(S/r)^2$ in the free energy density appears which is due to the splay deformation

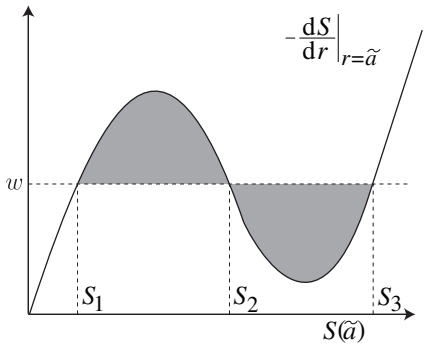

Figure 4. Generalized Maxwell construction for the prewetting transition close to a spherical particle. For a detailed explanation see the text.

in the radial director field. In a detailed investigation, we have shown that it quantitatively alters the prewetting transition in comparison with mean-field theories for a purely scalar order parameter where this term does not occur [24]. The respective bulk and surface Euler–Lagrange equations now read

$$\frac{d^2S}{dr^2} + \frac{2}{r}\frac{dS}{dr} - 6\frac{S}{r^2} - \frac{df_b(S)}{dS} = 0, \qquad \left.\frac{dS}{dr}\right|_{r=\tilde{a}} = -w. \tag{17}$$

We again want to determine the order-parameter profile $S(r)$ under the boundary condition $S(r \to \infty) = 0$. In particular, we are interested at the behaviour of $S(r = \tilde{a})$. However, compared with the planar case in equations (11), the spherical geometry creates two additional terms in the bulk equation so that it cannot be integrated once. This is illustrated by a mechanical analogy where we replace S and r by the spatial coordinate x and the time t, respectively. The bulk equation then describes the motion of a particle in a time-dependent potential and with a time-dependent friction coefficient for which energy conservation does not hold.

Following [9], we set up an alternative approach. We solve the bulk Euler–Lagrange equation of equations (17) for a fixed value $S(\tilde{a})$ at the particle surface. For the resulting order-parameter profiles, we can consider the derivative of $S(r)$ at the surface, $dS/dr|_{r=\tilde{a}}$, as a function of $S(\tilde{a})$. The same applies to the total free energy: $F = F(S(\tilde{a}))$. Since the order-parameter profiles satisfy the bulk Euler–Lagrange equation, one readily shows that

$$\frac{d[F(S(\tilde{a})) + wS(\tilde{a})]}{dS(\tilde{a})} = -\left.\frac{dS}{dr}\right|_{r=\tilde{a}} \tag{18}$$

or by integrating over S:

$$F(S(\tilde{a})) = \int_0^{S(\tilde{a})} \left(-\left.\frac{dS}{dr}\right|_{r=\tilde{a}} - w\right) dS. \tag{19}$$

The surface Euler–Lagrange equation in equations (17) is recovered for the value of $S(\tilde{a})$ that satisfies $dF(S(\tilde{a}))/dS(\tilde{a}) = 0$. The graphical solution of the surface equation is illustrated in figure 4 where we plot $-dS/dr|_{r=\tilde{a}}$ as a function of $S(\tilde{a})$. The intersections with the horizontal line at w give here three possible solutions for the surface value. From equation (19) it is clear that their free energies differ by the grey-shaded areas. The middle solution is a maximum, whereas in the example of figure 4 a phase transition between the other two solutions takes place since both areas agree. This is a generalized Maxwell construction. It determines a prewetting line (we have only one parameter in the surface potential). It ends in a critical point that occurs when $-dS/dr|_{r=\tilde{a}}$ as a function of $S(\tilde{a})$ possesses a saddle point.

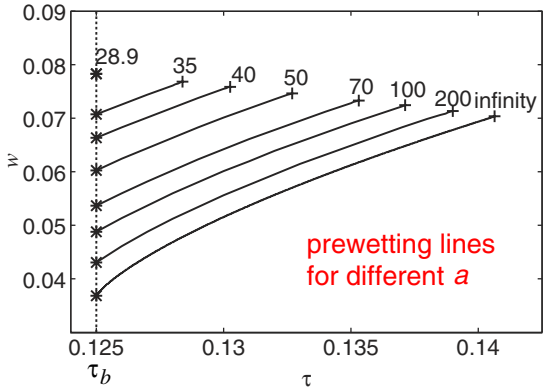

Figure 5. Wetting phase diagrams for different particle radii $\tilde{a}$. The prewetting line vanishes below a critical particle radius of $\tilde{a} = 28.9$ which corresponds to 100 nm.

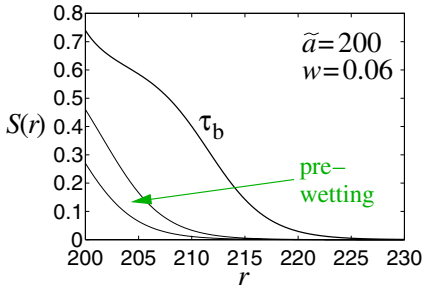

Figure 6. Order-parameter profiles for the reduced particle radius $\tilde{a} = 200$ and $w = 0.06$. The two lower curves show the transition from the thin-film to the thick-film solution when crossing the prewetting line. The upper curve belongs to the bulk phase-transition temperature τ_b.

In [24] we discuss in detail how $-\mathrm{d}S/\mathrm{d}r|_{r=\tilde{a}}$ as a function of $S(\tilde{a})$ behaves for different particle radii. As a final result, we arrive at the wetting phase diagrams illustrated in figure 5 for different particle radii a. The prewetting line for the planar case is given for an infinite particle radius. Note that due to numerical limitations, we cannot resolve the expected tangential approach to the coexistence line at $\tau = \tau_b$. The major result is that the prewetting line vanishes below a critical radius $a \approx 100$ nm. It is determined by the requirement that $-\mathrm{d}S/\mathrm{d}r|_{r=\tilde{a}}$ as a function of $S(\tilde{a})$ exhibits a saddle point at $\tau = \tau_b$. In figure 6, we finally illustrate various order-parameter profiles for a particle radius of $a = 700$ nm ($\tilde{a} = 200$) and $w = 0.06$. The lower two curves represent the profiles when the prewetting line is crossed and the upper curve is at the bulk phase transition. Clearly, the thickness of the wetting layer no longer diverges since this would mean that the free energy of the nematic–isotropic interface also diverges.

Our next step is to determine how the wetting layers change the Stokes drag of a colloidal particle compared with a simple Newtonian fluid. This could be a means to study details of the wetting scenario discussed above via dynamic light scattering which measures the Stokes friction coefficient via the Brownian motion of a colloidal particle.

Acknowledgments

The authors thank W Poon. Discussions with him on the Stokes drag of colloidal particles initiated this work. The authors also acknowledge helpful comments by D Cleaver

and the referees. HS thanks the Yokoyama Nano-structured Liquid Crystal Project for generous financial support during his stay in Tsukuba. He also acknowledges financial support from the Deutsche Forschungsgemeinschaft under grant no Sta 352/5-1.

References

[1] See the webpage: http://www.botanik.uni-bonn.de/system/bionik.htm
[2] Cahn J W 1977 *J. Chem. Phys.* **66** 3667
[3] Dietrich S 1988 *Phase Transitions and Critical Phenomena* vol 12, ed C Domb and J Lebowitz (London: Academic)
[4] Schick M 1990 *Liquids at Interfaces* (*Les Houches, Session XLVIII*) ed J Charvolin, J F Joanny and J Zinn-Justin (Amsterdam: Elsevier)
[5] Nakanishi H and Fisher M E 1982 *Phys. Rev. Lett.* **49** 1565
[6] Lipowsky R 1982 *Phys. Rev. Lett.* **49** 1575
[7] Lipowsky R and Speth W 1983 *Phys. Rev.* B **28** 3983
[8] Levinson P, Jouffroy J and Brochard F 1985 *J. Physique Lett.* **46** L-21
Holyst R and Poniewierski A 1987 *Phys. Rev.* B **36** 5628
Gelfand M P and Lipowsky R 1987 *Phys. Rev.* B **36** 8725
[9] Indekeu J O, Upton P J and Yeomans J M 1988 *Phys. Rev. Lett.* **61** 2221
Upton P J, Indekeu J O and Yeomans J M 1989 *Phys. Rev.* B **40** 666
[10] Bieker T and Dietrich S 1998 *Physica* A **252** 85
Evans R, Roth R and Bryk P 2003 *Europhys. Lett.* **62** 815
[11] Jérôme B 1991 *Rep. Prog. Phys.* **54** 391
[12] For a collection of references see, Lelidis I and Galatola P 2002 *Phys. Rev.* E **66** 010701(R)
[13] Sheng P 1982 *Phys. Rev.* A **26** 1610
[14] Poniewierski A and Sluckin T J 1984 *Mol. Cryst. Liq. Cryst.* **111** 373
Poniewierski A and Sluckin T J 1984 *Mol. Cryst. Liq. Cryst.* **126** 143
Poniewierski A and Sluckin T J 1987 *Liq. Cryst.* **2** 281
[15] Sluckin T J and Poniewierski A 1985 *Phys. Rev. Lett.* **55** 2907
Croxton C A (ed) 1986 *Fluid Interfacial Phenomena* (New York: Wiley)
[16] Borštnik A, Stark H and Žumer S 1999 *Phys. Rev.* E **60** 4210
Borštnik A, Stark H and Žumer S 2000 *Phys. Rev.* E **61** 2831
[17] Kočevar K and Muševič I 2001 *Phys. Rev.* E **64** 051711
[18] Kočevar K, Borštnik A, Muševič I and Žumer S 2001 *Phys. Rev. Lett.* **86** 5914
[19] Galatola P and Fournier J-B 2001 *Phys. Rev. Lett.* **86** 3915
Galatola P, Fournier J-B and Stark H 2003 *Phys. Rev.* E **67** 031404
[20] Stark H 2002 *Phys. Rev.* E **66** 041705
[21] Russel W B, Saville D A and Schowalter W R 1995 *Colloidal Dispersions* (Cambridge: Cambridge University Press)
[22] Fukuda J, Stark H and Yokoyama H 2004 *Phys. Rev. Lett.* submitted
[23] Böttger A, Frenkel D, van de Riet E and Zijlstra R 1987 *Mol. Cryst. Liq. Cryst.* **2** 539
[24] Fukuda J, Stark H and Yokoyama H 2004 *Phys. Rev.* E at press
[25] de Gennes P G 1971 *Mol. Cryst. Liq. Cryst.* **12** 193
[26] Nobili M and Durand G 1992 *Phys. Rev.* A **46** R6174
[27] Hauge E H and Schick M 1983 *Phys. Rev.* B **27** 4288